1

Morphology of Tumor Vasculature: A Theoretical Model

Katalin Bartha[1] and Heiko Rieger[2]

[1] Department of Medical Biochemistry, Semmelweis University, Budapest, Hungary katalin_bartha@puskin.sote.hu
[2] Theoretische Physik, Universität des Saarlandes, 66041 Saarbrücken, Germany h.rieger@mx.uni-saarland.de

Summary. A theoretical model based on the molecular interactions between a growing tumor and a dynamically evolving blood vessel network describes the transformation of the regular vasculature in normal tissues into a highly inhomogeneous tumor specific capillary network. The emerging morphology, characterized by the compartmentalization of the tumor into several regions differing in vessel density, diameter and degree of tumor necrosis, is in accordance with experimental data for human melanoma. Vessel collapse due to a combination of severely reduced blood flow and solid stress exerted by the tumor, leads to a correlated percolation process that is driven towards criticality by the mechanism of hydrodynamic vessel stabilization.

Key words: Tumors, angiogenesis, cooption, remodeling, blood flow, network morphology, fractals

1.1 Introduction

Tumor vasculature, the network of blood vessels in and around a growing tumor, is in many respects different from the regular vasculature in normal tissues. Hypoxia, the lack of oxygen, that prevents a small tumor nucleus from further growth, induces the expression of various diffusible growth factors (GF) by the tumor cells that trigger a coordinated response of angiogenesis - the formation of irregular blood vessels [1, 2]. The expected increase in microvasular density (MVD) is usually observed in the periphery of the tumor, whereas the morphology of the vasculature in the central part of the tumor is characterized by a *decreased* MVD, dilated vessels and regions of necrotic tumor tissue [3, 4]. The resulting tumor specific capillary network is very heterogeneous, composed of dense and void regions, and has a fractal dimension different from normal arterio-venous or normal capillary networks [5].

Although on the molecular level the main actors in the angiogenic game are rapidly identified, the physical principles that determine the global mor-

phology of the vascular network in tumor tissues are not known. Since for instance MVD is used as a diagnostic tool in cancer therapy [6] a quantitative understanding of the mechanism that leads to the compartmentalization of the tumor vasculature into various regions differing substantially in vessel density appears mandatory. Moreover, scale-invariant aspects like fractal dimension are used as hints towards the nature of the growth process underlying the formation of the tumor vasculature [7]. In this paper we propose a theoretical model for the evolution of tumor vasculature that illuminates the physical principles leading to its global morphology [8]. The experimentally observed increase in MVD at the tumor perimeter and periphery and decrease in MVD and vessel dilation in the tumor center in human melanoma [4] appear as the general scenario in our theoretical model. Furthermore, we will argue that vessel collapses in the interior of the tumor lead to a percolation process which is driven towards criticality, the percolation threshold, via a mechanism of vessel stabilization by increased blood flow in the remaining vessels.

1.2 Model

There is a large amount of work on the mathematical modeling of tumor-induced angiogenesis (for reviews see e.g. [9, 10]), which can be classified into two groups: Either they concentrate on blood vessel densities rather than vessel morphology (as in continuum partial differential equation [11, 12] or in locally-coupled map lattice [13] approaches), or they represent vessels as interconnected lattice patterns, line segments, or continuous curves [14, 15, 16, 17] and assume a static tumor. A growing tumor in the vascular phase, however, remodels the blood vessel network via cooption, regression and growth - and the emerging morphology is determined by the interaction of the two dynamically evolving systems: The growing tumor and the remodeling vessel network.

Vessel network
We describe the vessel network by a graph $G = (V, E)$, in which edges $e \in E$ represent tubular vessel segments of diameter $d(e)$ and nodes $v \in V$ represent vessel junctions, where two or more vessel segments join. For the moment we restrict to capillary networks and do not discriminate between arteries and veins, but a hierarchical structure of the original vessel network is easily incorporated into our model [18]. The network is fixed in an initial configuration representing features of the normal tissue vasculature like homogeneous microvascular density, typical vessel diameters etc., but it can dynamically change over time: new vessels can be inserted, others can be removed, vessel diameter can change. For computational simplicity we allow only discrete locations of the nodes, i.e. the occupy certain sites on a square lattice of grid size $10\mu m$, by which each node gets a Cartesian coordinate $\mathbf{r}(v) = (x, y)$.

Blood flow
Blood flow through this interconnected network of tubes is assumed to be an ideal pipe flow with flow conservation at all junctions v: $\sum_{e \in E(v)} q(e) = 0$, which is Kirchhoff's law. $E(v)$ is here the set of all edges attached to the node v, and $q(e)$ the flow rate through vessel e. $q(e)$ and $f(e)$, the the shear force $f(e)$ acting upon the vessel wall, then follow Hagen-Poiseuille's law:

$$q(e) = (\pi/128)\eta_{d(e)}^{-1} \cdot d^4(e)\ \nabla P(e) \quad \text{and} \quad f(e) = (1/4) \cdot d(e) \nabla P(e), \quad (1.1)$$

where $\nabla P(e)$ is the pressure gradient in e, which is $\nabla P(e) = P(v_1(e)) - P(v_2(e))/l(e)$, with $P(v)$ the pressure at node v, $v_1(e)$ and $v_2(e)$ the start and end points of the edges e, and $l(e)$ the length of vessel e. In principle the viscosity $\eta_{d(e)}$ depends on the tube diameter $d(e)$, since blood is a non-Newtonian fluid, but for simplicity we set it to a constant, as it is correct initially, when all vessels have the same diameter.

Together with fixed boundary condition for the blood pressure $P(v)$ the flow conservation equations establish an inhomogeneous system of linear equations for the blood pressures $P(e)$, which is solved numerically for the vessel network at hand. We choose boundary conditions that produces a homogeneous blood flow and shear stress in all capillaries in the initial network: $P(v)$ is fixed on all nodes v on the boundaries of the system such that it decreases linearly from $P_{\max}$ at the node at $\mathrm{r} = (x, y) = (L, L)$ along the boundary nodes at $\mathrm{r} = (L, y)$ and $\mathrm{r} = (x, L)$ to $(P_{\max} - P_{\min})/2$ at $\mathrm{r} = (L, 0)$ and $\mathrm{r} = (0, L)$; and from here further linearly along the boundary nodes at $\mathrm{r} = (x, 0)$ and $\mathrm{r} = (0, y)$ to $P_{\min}$ at $\mathrm{r} = (0, 0)$. One should not that this boundary conditions produces a pressure gradient and hence a global blood flow in the diagonal direction, which is somewhat unrealistic and will be repaired in initial network configurations that contain a hierarchy of arteries and veins.

Tumor growth
The tumor in our model is defined on a square lattice, where each site represents an area of $10\mu m \times 10\mu m$. The tumor configuration is given by the set of lattice sites T that are occupied by tumor cells. Initially a nucleus of N_0 sites is occupied by tumor cells, proliferation can happen only at empty neighbor sites of already occupied sites [19], removal (death) of tumor cells can happen everywhere. The restriction of tumor cell (TC) proliferation to the outer rim of the tumor is also observed in real tumors [20] and in theoretical models involving TC elasticity and increasing solid stress inside the tumor [21]. More sophisticated representations of the growing tumor are easily incorporated later into our model.

Oxygen concentration
Proliferation and death of tumor cells depend on the supply of oxygen (or other nutrients), which is determined by the current vessel network: Oxygen is transported by blood flow through the vascular system and has to diffuse through the vessel wall to reach other cells in the extracellular matrix. In case

of a highly diffusible solute like oxygen the transmural flux J_w is essentially driven by the difference between the oxygen levels inside and outside the vessel. With this boundary condition the distribution of extracellular oxygen is described by a diffusion equation with sink terms, for which the adiabatic approximation is completely sufficient [22, 23], since the inter-vessel diffusion time for oxygen is of the order of 1-10 seconds [24, 25] whereas the cell proliferation time is several hours.

The Green's function method is an elegant and computationally tractable way to solve the diffusion problem for the oxygen delivery to tissue by microvascular networks also for large grid sizes [27, 26]. The essential idea is to represent blood vessels as a set of discrete O_2 sources and the O_2 field in the tissue as a superposition of fields resulting from those sources. In the most general case the source and sink strengths are unknown and have to be determined implicitly by solving a system of linear equations for them.

Here we assume a uniform oxygen consumption rate M_0 of the normal tissue. Then the oxygen distribution at site $\mathbf{r}$ resulting from a unit point source at $\mathbf{r}'$ is defined as the Green's function $G(\mathbf{r}, \mathbf{r}')$ and given by the solution of

$$D\Delta_{\mathbf{r}} G - M_0 G = -\delta(\mathbf{r} - \mathbf{r}') \,, \tag{1.2}$$

where D is the oxygen diffusion constant and $\delta(\mathbf{r})$ is the delta function. The resulting $G(\mathbf{r}, \mathbf{r}')$ depends only on the distance from the point source $R = |\mathbf{r} - \mathbf{r}'|$ and decays exponentially with R on a length scale $R_{\text{oxy}} = \sqrt{D/M_0}$). For computational convenience we replace the exact Green's function by a piece-wise linear function that decays to zero on the same length scale:

$$G(\mathbf{r}, \mathbf{r}') = \frac{3}{\pi R_{\text{oxy}}^2} \left(1 - \frac{|\mathbf{r} - \mathbf{r}'|}{R_{\text{oxy}}}\right) \cdot \theta(|\mathbf{r} - \mathbf{r}'| - R_{\text{oxy}}) \,, \tag{1.3}$$

where $\theta(x)$ is the step function ($\theta(x) = 1$ for $x \geq 0$, $\theta(x) = 0$ for $x < 0$). Furthermore here we assume for simplicity that the presence of TCs does not significantly alter the oxygen consumption rate M_0. At least for melanoma this appears to be an acceptable approximation, since the skin tissue $\text{MVD}_0 \approx 100/mm^2$ [4] indicates $R_{\text{oxy}} \approx 100\mu m$ (see below), and data for pO_2 gradients in tumors also indicate $R_{\text{oxy}} \approx 100\mu m$ [1]. There are, however, various ways in which one could include the effect of an increased cell density approximatively, for instance by introducing a TC-density dependent O_2 diffusion range $R_{\text{oxy}}(\rho)$ that decreases monotonously with the local tumor-cell density ρ.

The total oxygen concentration $O_2(\mathbf{r})$ is then given by

$$O_2(\mathbf{r}) = \sum_{e \in E} \sum_{\mathbf{r}' \in e} J(\mathbf{r}') \cdot G(\mathbf{r}, \mathbf{r}'). \tag{1.4}$$

where $J(\mathbf{r}')$ is the source strength of a vessel segment with its center at $\mathbf{r}'$ [27]. This depends on the difference between the blood O_2 partial pressure inside the vessel segment at $\mathbf{r}'$, $P_{\text{oxy}}(\mathbf{r}')$, and the tissue O_2 concentration at

$\mathbf{r}'$: $J(\mathbf{r}') = P_{\mathrm{oxy}}(\mathbf{r}') - O_2(\mathbf{r}')$. Inserting this into (1.4) yields a system of linear equations for $O_2(\mathbf{r}')$ at all vessel segment $\mathbf{r}'$, its solution determines $J(\mathbf{r}')$. We implemented this procedure for various (small) vessel network configurations and compared the resulting field $O_2(\mathbf{r})$ with one that we obtained by setting $J(\mathbf{r}') = 1$ for all vessel segments $\mathbf{r}'$. It turned out that both models lead to qualitatively the same O_2 fields for the range of MVDs that occur in our simulation runs (see below). Quantitatively the model with constant source strengths overestimates the O_2 concentration by ca. 40% for inter-capillary distance of $0.5 \cdot R_{\mathrm{oxy}}$, corresponding to $2{\cdot}\mathrm{MVD}_0$. Hence for computational simplicity we assume constant source strengths $J(\mathbf{r}') = 1$ in our model.

Growth factor distribution
Tumor cells under hypoxia secret increased amounts of growth factors that can stimulate the formation of new blood vessels. In our model we assume that a TC at site $\mathbf{r}$ secrets GF if $O_2(\mathbf{r}) < c_{\mathrm{oxy}}$. The diffusion of the molecules into the extracellular matrix can be described by a diffusion process with source terms, which can again well be approximated to be adiabatic:

$$D_{\mathrm{GF}} \Delta GF(\mathbf{r}) - k_1 GF(\mathbf{r}) + s_{GF}(\mathbf{r}) = 0 \,, \tag{1.5}$$

where $GF(\mathbf{r})$ is the GF concentration field, D_{GF} is the diffusion constant for GF in the ECM, k_1 is the degradation rate of the growth factors and $s_{GF}(\mathbf{r})$ the source strength at location $\mathbf{r}$. The latter we assume to be a delta function of unit weight at each tumor cell under hypoxia. As a result this diffusion equation can again be solved by the Greens-function method and we replace the exact Greens function by a piecewise linear function as for the oxygen concentration field. The GF concentration therefore is

$$GF(\mathbf{r}) = \sum_{\mathbf{r}' \in T \text{ with } O_2(\mathbf{r}') < c_{\mathrm{oxy}}} \frac{3}{\pi R_{\mathrm{GF}}^2} \left(1 - \frac{|\mathbf{r} - \mathbf{r}'|}{R_{\mathrm{GF}}}\right) \cdot \theta(|\mathbf{r} - \mathbf{r}'| - R_{\mathrm{GF}}) \tag{1.6}$$

Dynamics
TCs proliferate/die when the local oxygen concentration is high/low. Vessels (edges) emerge when the local GF concentration is high enough, and they vanish (collapse) stochastically inside the tumor, when the hydrodynamic shear force acting on the vessel walls is too low. The biological and pathophysiological motivation for the details of the model definition is discussed in [8].

Starting with the initial configuration described above the following updates are performed sequentially in each time step of duration $\Delta t = 1h$, c.f. Fig. 1.1 for illustration.

(a) TC proliferation:
TCs can proliferate at tumor surface sites if the local oxygen concentration is sufficient: If $\mathbf{r}$ is not occupied by a TC but has at least one neighboring TC and if $O_2(\mathbf{r}) > c_{\mathrm{oxy}}$: $T \to T \cup \{\mathrm{r}\}$ with probability $p_{\mathrm{TC}}^{\mathrm{new}} = \Delta t / t_{\mathrm{TC}}$.

(b)TC death:
TCs that are extremely under-oxygenated for a long time are eliminated. We define the threshold for extreme under-oxygenation to be 10% of the threshold beyond which they start to proliferate (i.e. $0.1 \cdot c_{\rm oxy}$). If $O_2(\mathbf{r}) < 0.1 c_{\rm oxy}$ for a TC at site $\mathbf{r}$ the counter for the time that a TC at site $\mathbf{r}$ spent in hypoxia is increased by one: $t_{\rm uo}(\mathbf{r}) \to t_{\rm uo}(\mathbf{r}) + 1$. When $t_{\rm uo}(\mathbf{r}) > t_{\rm max}$, the TC is eliminated: $T \to T - \{\mathbf{r}\}$ with probability $p_{\rm TC}^{\rm death} = 1/2$.

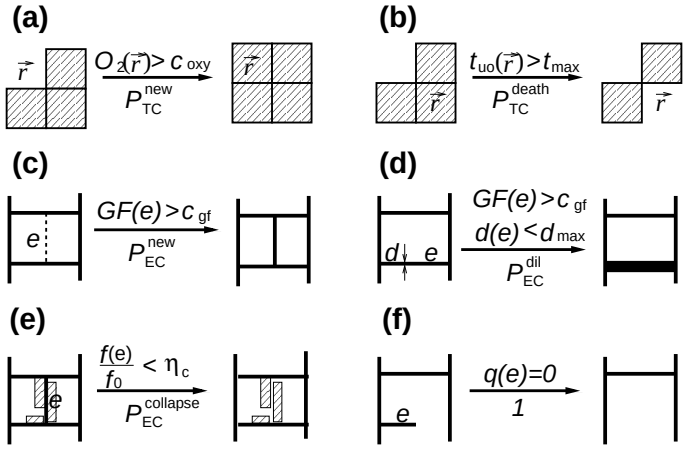

Fig. 1.1. Schematic illustration of the model: (a) TC proliferation, (b) TC death, (c) Vessel growth, (d) Vessel dilatation, (e) Vessel collapse due to low shear force, and (f) Collapse of non-circulated vessels.

(c) Vessel growth:
New straight vessel segments between two circulated vessels at site $\mathbf{r}$ and $\mathbf{r'}$ are introduced with probability $\Delta\tau/T_e$ (where T_e is the EC proliferation time) if: $GF(\mathrm{r}, t) > c_{\rm GF}$, the neighbor of $\mathbf{r}$ on the migration path is not occupied by a TC, no site and no neighbor site of the migration path is occupied by ECs except $\mathbf{r}$ and $\mathbf{r'}$, and $|\mathbf{r} - \mathbf{r}'| < M_{\rm max}$ ($M_{\rm max}$ being the maximum sprout migration distance). In case of such an event $e(\mathbf{r}, t) = 1$ and $e_r(\mathbf{r}, t) = r_0$ along this path, and $O_2(\mathbf{r}, t)$ is updated.

(d)Vessel dilatation:
In our model a vessel segments e at site $\mathbf{r}$ that is surrounded by TCs and has a GF concentration $GF(\mathbf{r}, t)$ larger than $c_{\rm GF}$ increase its radius $d(e)$ by an amount $r_0/2\pi$ with probability $\Delta\tau/T_e$ as long as $d(e) \le d_{\rm max}$. To mimic the smoothening effect caused by the surface tension of the vessel walls the location of the dilation is shifted to a neighboring vessel segment if a radius difference larger than $r_0/2\pi$ would arise at the original location.

(e+ f) Vessel regression and collapse:
Vessels can collapse due to solid stress exerted by the tumor and also long-

term reduction of wall shear stress is associated with a dramatic reduction of the vessel diameter, up to complete vessel occlusion. We used both criteria to identify critical vessels: weakly perfused vessels e, which are surrounded by TCs, collapse with probability $p = \Delta\tau/_{\mathrm{Tcollapse}}$ if the wall shear stress $f(e)$ is below a critical value f_{crit} [26]. After each collapse event the blood flow is re-computed and $O_2(\mathbf{r}, t)$ is updated. Vessels that are cut from the blood circulation ($q(e) = 0$) are instantaneously removed.

1.3 Results

In contrast to [8] we consider here a situation in which the MVD of the original vessel network is not sufficient for the tumor cells to proliferate and the secretion of GF is necessary to increase the MVD such that TCs can proliferate in certain regions of the tumor.

The original vasculature is modeled by a regular network of capillaries in a Manhattan pattern with vessel-to-vessel distance $\delta = 100\mu m$. This implies that the original MVD is 10 vessel per mm (measured by counting the number of vessels in a vertical cut). If we extend the network into 3 dimensions with the same network parameters this implies a MVD of $100/\mathrm{mm}^2$, close to the value that is characteristic for skin tissue [4]. With $R_{\mathrm{oxy}} = 100\mu m$ this yields an oxygen concentration that is nearly homogeneous and has a value of $\overline{O}_2 = 0.2$ (measured in the source strength of each vessel segment). Thus setting $c_{\mathrm{oxy}} = 0.3$ implies that TCs can survive (since according to our definition they die only their oxygen supply falls below $0.1c_{\mathrm{oxy}} = 0.03$), but cannot proliferate in the original network.

We set R_{GF} to $150\mu m$. The value of c_{GF} is not crucial, if it is low it implies that new vessels can be generated within nearly the whole radius R_{GF} around a GF secreting TC. We set it to $c_{\mathrm{GF}} = 0.01$. Cells proliferate on the time scale of several hours, therefore we set the time step to $\Delta\tau = 1h$. Other parameters are: Collapse probability $\Delta\tau/T_{\mathrm{collapse}} = 0.01$, critical shear force $f_{\mathrm{crit}} = 0.5f_0$ (where f_0 is the shear force in the original vasculature), sprout generation time $T_e = 40h$, TC proliferation time $T_c = 10h$, maximum sprout distance $M_{\mathrm{max}} = 100\mu m$, TC-survival time to $t_{\mathrm{max}} = 100h$, maximum vessel radius to $d_{\mathrm{max}} = 35\mu m$ [4] and size of the initial tumor nucleus $N_0 = 1000$.

To obtain data for the stochastic time evolution of our model according to the dynamics defined above we performed Monte Carlo simulations. The result of one representative run is shown in Fig. 1.2.

Tumor/vessel configurations at different times are shown in the middle column of Fig. 1.2: Starting from a regular vessel network the MVD in the peritumoral region is increased due to the supply of GFs from the tumor. Once the tumor grows over this highly vascularized region, vessels start to collapse, by which the MVD tumor center is continuously decreased until only a few thick vessels, surrounded by cuffs of TCs remain. TCs in a distance larger than R_{oxy} from these vessel die after time t_{max} producing necrotic regions.

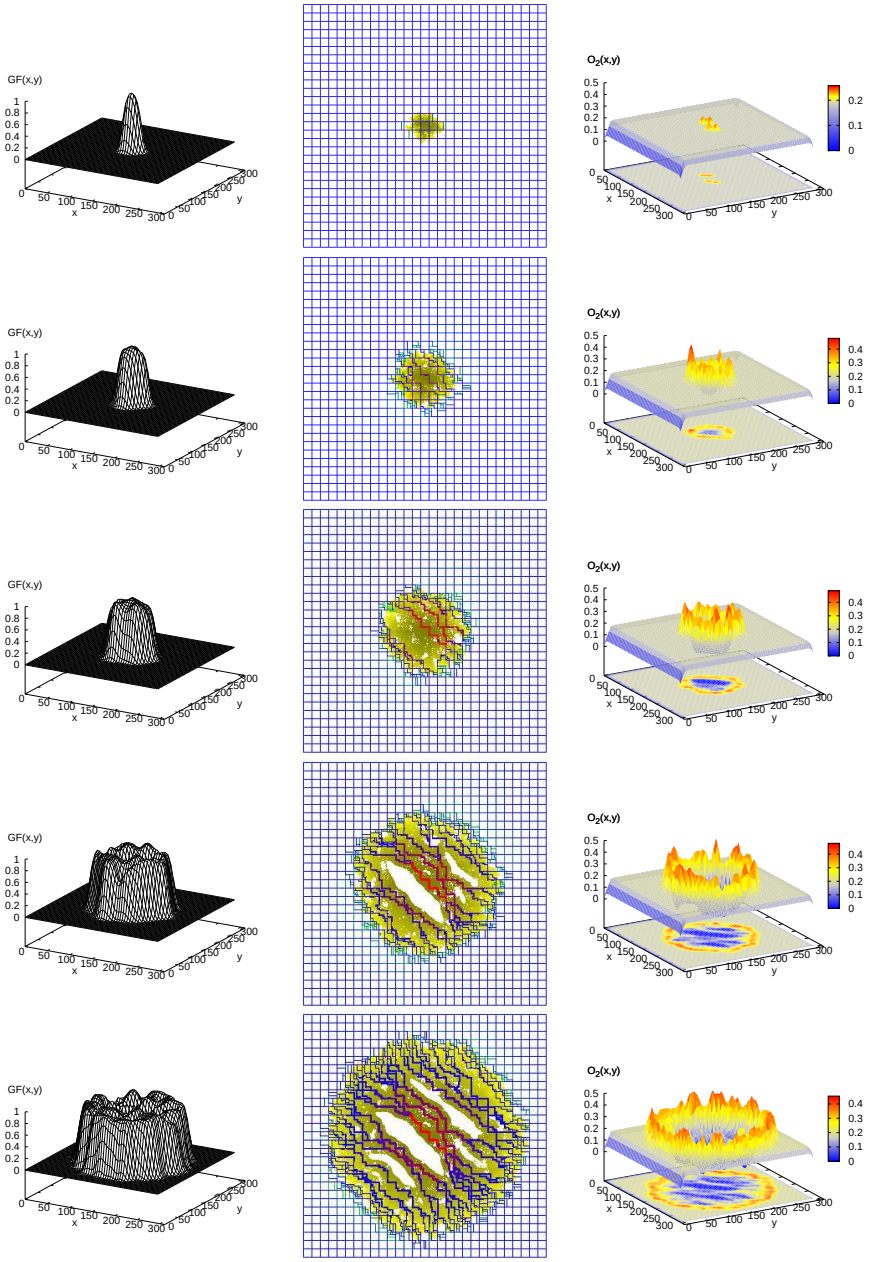

Fig. 1.2. Middle panel: Tumor and vessel network configuration at time $t = 1$, 100, 200, 400 and 600 (from top to bottom). The tumor is the grey area in the center - older TCs are darker than younger ones. The initial capillary network can be seen at $t = 1$ (with a few new vessels already there) vessel-to-vessel distance is $100\mu m$. White areas are necrotic regions. **Left and right panel:** GF and oxygen concentration, respectively, for the configurations in the middle panel.

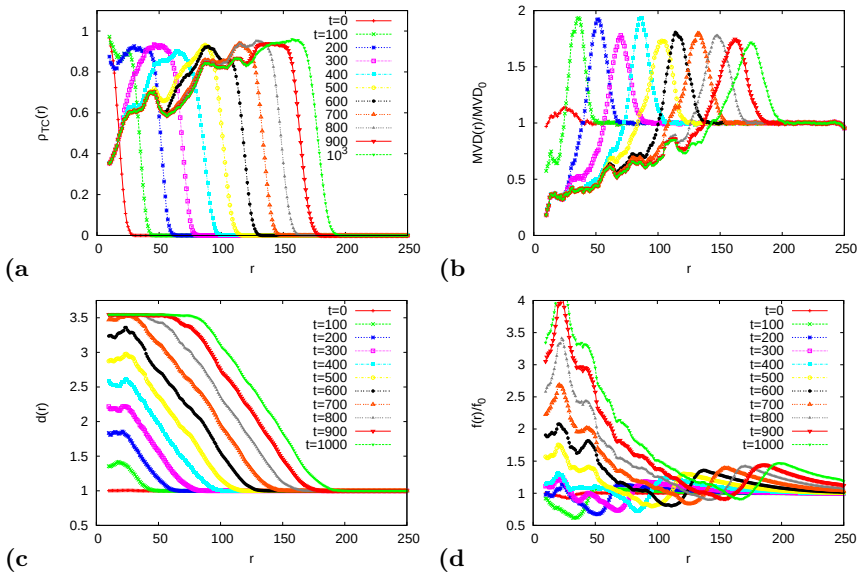

Fig. 1.3. **(a:** Tumor density as a function of the distance r from the tumor center for different equidistant times t. One sees clearly that the radius of the tumor grows linearly in time. **(b:** $\mathrm{MVD}/\mathrm{MVD}_0$ as a function of r for different equidistant times t (same symbols as in (a)). By comparison with the plots for tumor density in (a) one sees that the maximum MVD is localized at the tumor boundary, where it is up to 2 times larger than in the normal tissue. **(c):** Vessel diameter: It starts to increase linearly with decreasing r at the tumor boundary. For a fixed r below the actual tumor radius the average vessel radius increases linearly with time. **(d):** Shear force acting on the vessel walls, normalized to the shear force in the original capillaries. Note the pronounced dip: It is located at the maximum of the MVD in b, i.e. at the tumor boundary: This is also the region where most vessels will collapse.

The left and right column of Fig. 1.2 show the GF concentration $GF(x, y)$ and oxygen concentration $O_2(x, y)$, respectively, for the tumor/vessel configurations at time t. Both indicate roughly the spatial extend of the tumor and the region where new vessels can grow. Far away from the tumor it is $O_2(\mathbf{r}) = \overline{O}_2 = 0.2$ and only in the peritumoral region it is $O_2(\mathbf{r}) > c_{oxy} = 0.3$. Inside the tumor $O_2(\mathbf{r})$ is drastically reduced at later time, leading to underoxygenation of TCs and thus to GF production. Consequently inside the tumor $GF(\mathbf{r})$ is high, nearly one everywhere - except in the necrotic regions. Fig. 1.2 indicates a compartmentalization of the tumor into different shells characterized by MVD, vessel diameter and necrosis, as observed in real tumors [4]: A highly vascularized peritumoral regions, a well oxygenated tumor periphery and an hypoxic tumor center with decreased MVD, increased vessel diameter, and large necrotic regions.

Figure 1.3 presents a quantitative analysis of this dynamical evolution. Shown in Fig. 1.3(a) is the radial tumor density $\rho_{\rm TC}(R)$. The tumor radius grows linearly with time t: $R_{\rm TC}(t) - R_{\rm TC}(0) \simeq 2t/t_{\rm TC}$, where the factor 2 is typical for the Eden growth. The radial vessel density $MVD(R)$, shown in Fig. 1.3(b) is maximal at the tumor boundary at $R_{\rm TC}(t)$. With increasing time both densities are substantially reduced inside the tumor indicating the emergence of necrotic regions. The radial vessel diameter $d(R)$, shown in Fig. 1.3(c), increases linearly from 1 at $R \simeq R_{\rm TC} + R_{\rm GF}$ to $d_{\rm max}$ at the tumor center due to the continuous exposure of vessels to GF.

Such a characteristic vessel morphology is also in a quantitative agreement with experimental data presented in [4], where the morphometry of human malignant melanoma was analyzed and data for MVD and vessel perimeter were obtained in three different regions of the tumors: (I) the tumor center, (II) the tumor periphery - a 100μm wide band of tumor immediately adjacent to the invasive edge; and (III) the peritumoral host tissue - a 200μm wide band of host connective tissue immediately adjacent to the tumor periphery. It was found that for melanoma larger than 1.5mm the MVD in (I) was less than 50% of the normal tissue $\rm MVD_0$, in (II) it was ca. 50% more than $\rm MVD_0$, and in (III) it was ca. two times $\rm MVD_0$. Within the statistical error of the experimental data (up to 30%), this agrees reasonably well with our results.

We investigated extensively in how far our conclusions depend on the parameters chosen here – a full account of this parameter dependence is reported in [8]. It turns out that the model behavior is robust and the parameters can be changed over a wide range without changing the qualitative results, in particular: the characteristic compartmentalization of the tumor, the vessel network morphology, the fractal dimension (to be studied below) and others. The question arises, which simplifications are crucial and what would change our conclusions, if they are abandoned in favor of a more realistic description. Obviously we cannot deal with all of them at once here, but we name a few:
a) *Oxygen diffusion:* We modeled O_2 diffusion also by determining the source strength of each vessel implicitly as described in [27], also taking into account a TC density dependent O_2 consumption . Although this implies a major computational effort the quantitative change in the data (for fixed parameters) is only minimal - none of our conclusions is altered.
b) *Growth factor diffusion:* Passive (as we assumed in our model) or active (via concentration gradients) diffusion changes the effective diffusion range ($\rm R_{GF}$) slightly, but does not alter our conclusions.
c) *Radius dependent viscosity:* (to model the Fahreus-Linquist effect) does not change our results, as we checked.
d) *Tumor growth:* More sophisticated tumor growth models can be incorporated than the simplified (Eden-growth inspired model) we use. We do not expect changes in our results as long as the tumor growth is restricted to a limited other shell of TCs (as theoretically described in [21] and experimentally reported in [20]).

More serious assumptions are those of a regular network of original capillaries, including the boundary conditions for the pressure we have chosen. We are currently working on a version of the model that starts with a hierarchical arterio-venous network [18], preliminary results indicate that the global picture that we present is maintained. Many other modifications are imaginable and will be studied in the future by us.

1.4 Fractal dimension

The geometrical features of the emerging tumor vasculature in our model are obviously very different from the original, regular capillary network: It consists of a combination of dense and void regions that might possess fractal properties. We used the box-counting method to determine the fractal dimension D_f as $N_\epsilon \sim \epsilon^{-d_f}$ where N_ϵ is the number of boxes of volume ϵ^2 necessary to cover the tumor vessel network, that is defined to lie within the outer limit of the peritumoral region. The plot of N_ϵ versus ϵ shown in Fig. 1.4 yields $d_f = 1.85 \pm 0.05$, which agrees with the value for the percolation cluster in conventional percolation in two dimension [28]. We get the same value for a wide range of parameter values and also with other methods to estimate d_f. When we restrict the fractal analysis to concentric shells ($R_1 \leq R \leq R_2$) the estimates for d_f decrease systematically decreasing the tumor center (see inset Fig. 1.4), reflecting the characteristic compartmentalization of the tumor vasculature also in the fractal properties.

Since d_f agrees with the value for the percolation cluster in $2d$ we conclude that the basic mechanism responsible for the fractal properties of the tumor vasculature in our model is the stochastic removal of vessels via vessel collapse and regression. In conventional percolation a critical cluster only emerges for an exactly tuned bond concentration. In our model the network is dynamically driven into this critical state without such a fine tuning since the removal of vessels is correlated with the blood flow: the collapse of weakly perfused vessels stabilizes the remaining ones due to an increase in blood flow. We propose that this mechanism is also at work in real tumors. Indeed the fractal analysis of two-dimensional photographs of vessel networks in human carcinoma yields a value of $D_f = 1.89 \pm 0.04$ [5], which agrees with d_f for the percolation cluster in $2d$ random percolation [28]. It has been suggested [5] that the origin of the fractal architecture of tumor vasculature might be based on an underlying invasion percolation process of the newly grown tumor vessels [29] due to inhomogeneities in the growth supporting matrix. Our theoretical model does not involve any such matrix-inhomogeneities and we propose that it is rather the flow correlated percolation process that determines the fractal properties of the tumor vasculature. Neo-vascularization mainly occurs at the tumor perimeter and a drastic reduction of vessel density is commonly observed in the interior of the tumor, therefore it appears unlikely that the fractal properties attained during growth in the periphery, independent of having

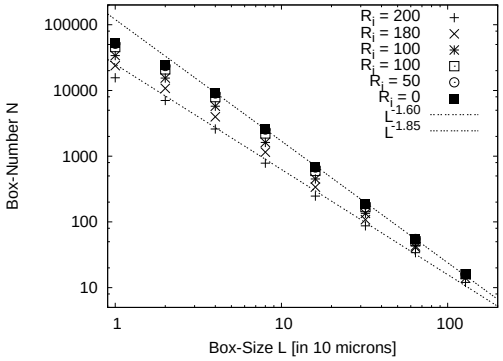

Fig. 1.4. Determination of the fractal dimension d_f of the vessel network at time $t = 1000$ via the box-counting method: The number of Boxes of size L that is needed to cover completely the vasculature is plotted as a function of L in log-log scale. The slope d_f of the curve is the fractal dimension. We confined the measurement to annuls with fixed outer radius that is determined by the limit of the peritumoral plexus and with varying inner radius R_i. The slope of the curves decreases with increasing R_i: $d_f = 1.85 \pm 0.05$ for $R_i = 0$ (full squares, which corresponds to the complete tumor vasculature) and $d_f = 1.60 \pm 0.05$ for $R_i = 200$ (which corresponds to the peritumoral plexus exclusively), indicating that the fractal dimension is not a homogeneous measure over all regions of the tumor vasculature.

characteristics of invasion percolation or not, survive the random dilution process in the tumor center. Thus, whereas in the proposal of [5] the fractal properties of the network are attained during *growth* of new vessels, we propose that it is mainly the *regression* of vessels that is responsible for the overall fractal morphology of the tumor vasculature.

1.5 Discussion

We have introduced a theoretical model for a dynamically evolving, two-dimensional vessel network interacting with a growing tumor, which is guided by experimental data for human melanoma. The emerging network morphology agrees well with those data and we find that the network is remodeled from a regular into a fractal structure with characteristics of conventional percolation. We have implemented the model also in three space dimensions and find similar results [30], where $d_f = 2.52$ turns out to correspond to $3d$ percolation. This suggests also for a large class of real solid tumor with decreased central MVD that the basic mechanism leading to the fractal features of the tumor vasculature is the random vessel collapse inside the tumor and not a stochastic vessel growth process.

An indirect experimental verification of this proposition is already given by the experimental data presented in [5, 7]: The fractal dimension of in-

vasion percolation (growth based mechanism), is 1.81 [29], whereas that of conventional percolation (collapse based mechanism) is 1.891 [28]. Their data for the fractal dimension the carcinoma vasculature is 1.88+/-0.02, which is obviously closer to, if not identical with, conventional percolation indicitaing at a collapse based mechanism.

A direct proof of the proposition that vessel collapse is the relevant mechanism that leads to the fractal structure of the tumor vasculature is probably difficult but at least imaginable: We hypothesize that stabilization of tumor vessels without hampering the growth of new vessels could give evidence for one or the other picture.

Antiangiogenic therapies with recurrent tumor growth may represent such a situation. Antiangiogenic blockade is known to lead to initial inhibition of vessel growth but also to vessel stabilization and tumors may resume growth if the blockade continues for extended period [31]. One of the possible mechanisms to such recurrence is the survival of some blood vessels which are stabilized by the adjacent smooth muscle cells and which survive VEGF withdrawal, while other small vessels lacking vascular supportive cells collapse. Despite the upregulation of VEGF (possibility for new vessel growth) observed in all such tumors that resumed growth during prolonged antiangiogenesis, new capillaries were not detected in any. Instead large central vessels with significantly increased diameters and increased smooth muscle developed. If the structural characteristics of vessel network formation were growth dependent (according to [5, 7]) the newly synthetized VEGF and sprouting would result in growth dependent scale invariance, but this was not the case. Therefore the study of the fractal properties of tumor vasculature after antiangiogenic treatment could proof that in the long term vessel collapse is the relevant mechanism that leads to the fractal structure of the tumor vasculature.

Acknowledgements: We thank Balázs Döme, Haymo Kurz and Sándor Paku for their input and discussions. This study was supported by the Hungarian Grant OTKA T-37454.

References

1. P. Carmeliet and R.K. Jain, Nature **407**, 249 (2000).
2. T. Acker and K.H. Plate, J. Mol. Med. **80**, 562 (2002).
3. J. Holash *et al.*, Science **284**, 1994 (1999); J. Holash, S.J. Wiegand, and G.D. Yancopoulos, Oncogene **18**, 5356 (1999).
4. B. Döme, S. Paku, B. Somlai, J. Tímár, J. Path. **197**, 355 (2002).
5. Y. Gazit *et al.*, Phys. Rev. Lett. **75**, 2428 (1995); J.W. Bais and R. K. Jain, Nature Med. **4**, 984 (1998).
6. L. Hlatky, P. Hahnfeld, and J. Folkman, J. Nat. Canc. Inst. **94**, 883 (2002).
7. J.W. Baish and R.K. Jain, Canc. Res. **60**, 3683 (2000).
8. K. Bartha and H. Rieger, J. Theor. Biol. **241**, 903 (2006); http://arxiv.org/abs/q-bio.TO/0506039 (2005).

9. N.V. Mantzaris, S. Webb, and H. G. Othmer, J. Math. Biol. **49**, 111 (2004).
10. *Cancer Modelling and Simulation*, edited by L. Preziosi (Chapman & Hall/CRC, Boca Raton, 2003).
11. H. M. Byrne and M. A. J. Chaplain, B. Math. Biol. **57**, 461 (1995).
12. H.A. Levine, B.D. Sleeman, and M. Nilsen-Hamiltion, J. Math. Biol. **42**, 195 (2001).
13. B. Capogrosso Sansone, M. Scalerandi, and C. A. Condat, Phys. Rev. Lett. **87**, 128102 (2001).
14. A.R.A. Anderson and M.A.J. Chaplain, Bull. Math. Biol. **60**, 857 (1998).
15. S. R. McDougall, A. R. A. Anderson, M. A. J. Chaplain, and J. A. Sherrat, B. Math. Biol. **64**, 673 (2002).
16. S. Tong and F. Yuan, Microvasc. Res. **61**, 14 (2002).
17. S. Y. Sun, M. F. Wheeler, M. Obeyesekere, and C. W. Patrick, B. Math. Biol. **67**, 313 (2005).
18. M. Welter, K. Bartha, H. Rieger, in preparation.
19. A.-L. Barabási and H. E. Stanley, *Fractal concepts in surface growth* (Cambridge University Press 1995).
20. A. Brú, S. Albertos, J. L. Subiza, J. L. Garca-Asenjo, I. Brú, Biophys. J. **85**, 2948 (2003).
21. D. Drasdo and S. Höme, Phys. Biol. **2**, 133 (2005).
22. A. A. Patel, E. T. Gawlinsky, S. K. Lemieux, and R. A. Gatenby, J. Theor. Biol. **213**, 315 (2001).
23. T. Alarcon, H.M. Byrne, and P.K. Maini, J. Theor. Biol. **225**, 257 (2003).
24. The diffusion constant of oxygen in tissue is of the order of $D \sim 10^{-5} cm^2/sec$ [25] and the mean square displacement of the underlying Brownian motion of the O_2-molecules is $\langle x^2(t) = Dt \rangle$, hence the mean time for O_2 to pass from one vessel to another which are $a = 100\mu m$ apart is ca. $\sqrt{a/D} = 10sec$.
25. A. S. Popel, Crit. Rev. Biomed. Eng. **17**, 257 (1989)
26. R. Gödde and H. Kurz, Dev. Dyn. **220**, 387 (2001).
27. R. Hsu, T. W. Secomb, Math. Biosci. **96**, 61 (19989); T. W. Secomb, R, Hsu, E. Y. H. Park, and M. W. Dewhirst, Ann. Biomed. Eng. **32**, 1519 (2004).
28. D. Stauffer and A. Aharony, *An introduction to Percolation Theory*, revised 2nd ed. (Taylor and Francis, London, 1994); C.D. Lorenz and R.M. Ziff, Phys. Rev. E **57**, 230 (1998).
29. L. Furuberg, J. Feder, A. Aharony, and T. Jossang, Phys. Rev. Lett. **61**, 2117 (1988). A.P. Sheppard, M.A. Knackstedt, W.V. Pinczewski and M. Sahimi, J. Phys. A **32**, L521 (1999).
30. D. S Lee, H. Rieger, and K. Bartha, Phys. Rev. Lett. **96**, 058104 (2006); http://arxiv.org/abs/q-bio.TO/0507043 (2005).
31. J. Z. Huang et al., Mol.Canc. Res. **2**, 36 (2004).